PNAS RESEARCH ARTICLE | BIOPHYSICS AND COMPUTATIONAL BIOLOGY
MICROBIOLOGY

Slower swimming promotes chemotactic encounters between bacteria and small phytoplankton

Riccardo Foffi[a], Douglas R. Brumley[b], François J. Peaudecerf[c], Roman Stocker[a], and Jonasz Słomka[a,1]

Affiliations are included on p. 11.

Edited by Lisa Fauci, Tulane University, New Orleans, LA; received June 6, 2024; accepted December 6, 2024

Chemotaxis enables marine bacteria to increase encounters with phytoplankton cells by reducing their search times, provided that bacteria detect noisy chemical gradients around phytoplankton. Gradient detection depends on bacterial phenotypes and phytoplankton size: large phytoplankton produce spatially extended but shallow gradients, whereas small phytoplankton produce steeper but spatially more confined gradients. To date, it has remained unclear how phytoplankton size and bacterial swimming speed affect bacteria's gradient detection ability and search times for phytoplankton. Here, we compute an upper bound on the increase in bacterial encounter rate with phytoplankton due to chemotaxis over random motility alone. We find that chemotaxis can substantially decrease search times for small phytoplankton, but this advantage is highly sensitive to variations in bacterial phenotypes or phytoplankton leakage rates. By contrast, chemotaxis toward large phytoplankton cells reduces the search time more modestly, but this benefit is more robust to variations in search or environmental parameters. Applying our findings to marine phytoplankton communities, we find that, in productive waters, chemotaxis toward phytoplankton smaller than 2 μm provides little to no benefit, but can decrease average search times for large phytoplankton (∼20 μm) from 2 wk to 2 d, an advantage that is robust to variations and favors bacteria with higher swimming speeds. By contrast, in oligotrophic waters, chemotaxis can reduce search times for picophytoplankton (∼1 μm) up to 10-fold, from a week to half a day, but only for bacteria with low swimming speeds and long sensory timescales. This asymmetry may promote the coexistence of diverse search phenotypes in marine bacterial populations.

chemotaxis | encounter rates | bacteria–phytoplankton interactions | microbial ecology

Significance

Microscale interactions between bacteria and phytoplankton impact nutrient cycling in the ocean. Chemotaxis can aid bacteria in navigating the gradients of chemicals exuded by phytoplankton cells, yet these gradients can often be noisy, and the type of noise experienced by chemotactic bacteria depends on the size of the phytoplankton cell. Combining the size dependence of the limits of chemotactic detection and cell–cell encounters, we show that bacteria searching for phytoplankton can benefit the most from chemotaxis toward small rather than large cells. We also find that fast swimming boosts chemotactic encounters with large phytoplankton, whereas slow swimming boosts chemotactic encounters with small phytoplankton. This size-dependent asymmetry of chemotactic performance may promote a diversity of search phenotypes in marine bacteria.

Chemotaxis, the ability to navigate chemical gradients, is often used by marine bacteria to navigate toward phytoplankton cells (1) and can be important for establishing symbiotic relationships and favoring metabolic exchanges which lie at the heart of the oceans' carbon cycles (2, 3). In the water column, phytoplankton cells generate chemical gradients by leaking dissolved organic compounds that can be strong attractants for bacteria (4, 5). The region immediately surrounding a phytoplankton cell where organic compounds are present in higher concentration, known as the phycosphere, acts as an ecological interface for the interactions between phytoplankton and bacteria (6). The composition of marine phytoplankton communities, which span more than two orders of magnitude in cell size from ∼0.5 μm to hundreds of micrometers (7), exposes bacteria to gradients on a wide range of lengthscales and amplitudes.

Swimming bacteria perform chemotaxis by sensing temporal changes in the concentration of chemoattractants and biasing their motility toward regions where chemoattractant concentrations are higher (8–10). Because it is based on a molecule-counting process, chemotaxis is inherently subject to noise (11, 12), especially at the low attractant concentrations typical of marine environments (13). The limits that noise imposes on chemosensing are well characterized for concentration fields with large spatial extent (14), most similar in the ocean to those generated by large phytoplankton, and for strong but short-lived pulses, representative for example of cell lysis events in the sea (15, 16). By contrast, our understanding of bacterial chemotaxis toward small phytoplankton cells, which generate sharp gradients tightly confined in space, is very limited, despite the disproportionate abundance in the ocean of small compared to large phytoplankton cells (17, 18). For instance, in a typical phytoplankton community in oligotrophic waters, more than 95% of the population is in the size range between 0.5 and 3 μm, and considerably less than 1% of phytoplankton cells are larger than 10 μm. Historically, less attention has been reserved to chemotaxis toward small

Author contributions: R.F., R.S., and J.S. designed research; R.F. and J.S. performed research; R.F. and J.S. analyzed data; R.F. implemented the simulation and analysis software and curated the data; and R.F., D.R.B., F.J.P., R.S., and J.S. wrote the paper.

The authors declare no competing interest.

This article is a PNAS Direct Submission.

[1]To whom correspondence may be addressed. Email: jslomka@ethz.ch.

This article contains supporting information online at https://www.pnas.org/lookup/suppl/doi:10.1073/pnas.2411074122/-/DCSupplemental.

Published January 10, 2025.

phytoplankton after a seminal computational study, though based on parameters determined for the enteric bacterium *Escherichia coli*, established that the gradients generated by phytoplankton cells with radii smaller than 3 to 4 μm could not be sensed by a swimming bacterium (19). This view has been recently overturned by NanoSIMS experiments, which revealed that chemotaxis confers an increased nutrient uptake to the marine bacterium *Marinobacter adhaerens* in the presence of the picocyanobacterium *Synechococcus* (20), demonstrating that bacterial chemotaxis toward the smallest and most abundant phytoplankton cells in the ocean is possible. Additionally, the swimming speed of bacteria affects both the signal and the noise in their measurement of chemical gradients (21) and spans more than one order of magnitude (10 to 100 μms^{-1}) in marine bacteria (22–24). These results underscore the importance of quantifying the impact of phytoplankton size and bacterial swimming speed on bacterial chemotactic performance, which we address in this study.

The Role of Phytoplankton Size in Chemotactic Searches

Phytoplankton cells of different sizes generate chemical gradients of different steepness and spatial extent, posing fundamentally different gradient detection challenges for bacteria. Bacteria experience chemical concentration fields in the form of temporal sequences of molecular adsorption events, which they integrate over a sensory timescale T to form an estimate of the local concentration gradient (11). An intuitive understanding of the problem can be obtained by comparing the adsorption sequences experienced by a bacterium moving in the chemoattractant fields generated by a large and a small phytoplankton cell (Fig. 1; see also discussion in *SI Appendix*). When moving in the chemoattractant field generated by a large phytoplankton cell, which is typically characterized by a large spatial extent and a shallow gradient, a bacterium will experience a large baseline adsorption rate with only a modest increase over subsequent sensory windows T as it nears the phytoplankton (Fig. 1 *A* and *C*). Detection of such gradients can fail if the gradient is too shallow and gets masked by the fluctuations inherent in the molecular adsorption events (14). By contrast, in the case of a small phytoplankton cell the concentration field is typically weaker and tightly localized in space: the signal will thus be indistinguishable from the background until the bacterium is in very close proximity to the phytoplankton, when it will experience a sharp increase in the rate of molecular adsorption events within a short time (Fig. 1 *B* and *D*). Detection of such gradients can fail as a result of the dynamic noise which arises from the combined effect of bacterial motion and the finite sensory timescale T: even though the gradients are steep and much less masked by fluctuations, they might not be detected because they occur over timescales smaller than the time required by the bacterium to process the signal. Such resolution limitations are inherent to any measurement system characterized by a finite processing time (25), including the bacterial chemotaxis pathway which is known to act as a low-pass filter (26, 27), but their effect on bacterial chemotaxis toward phytoplankton has remained unexplored. Furthermore, not only does the type of noise change as phytoplankton size decreases, but so does the nature of ran-

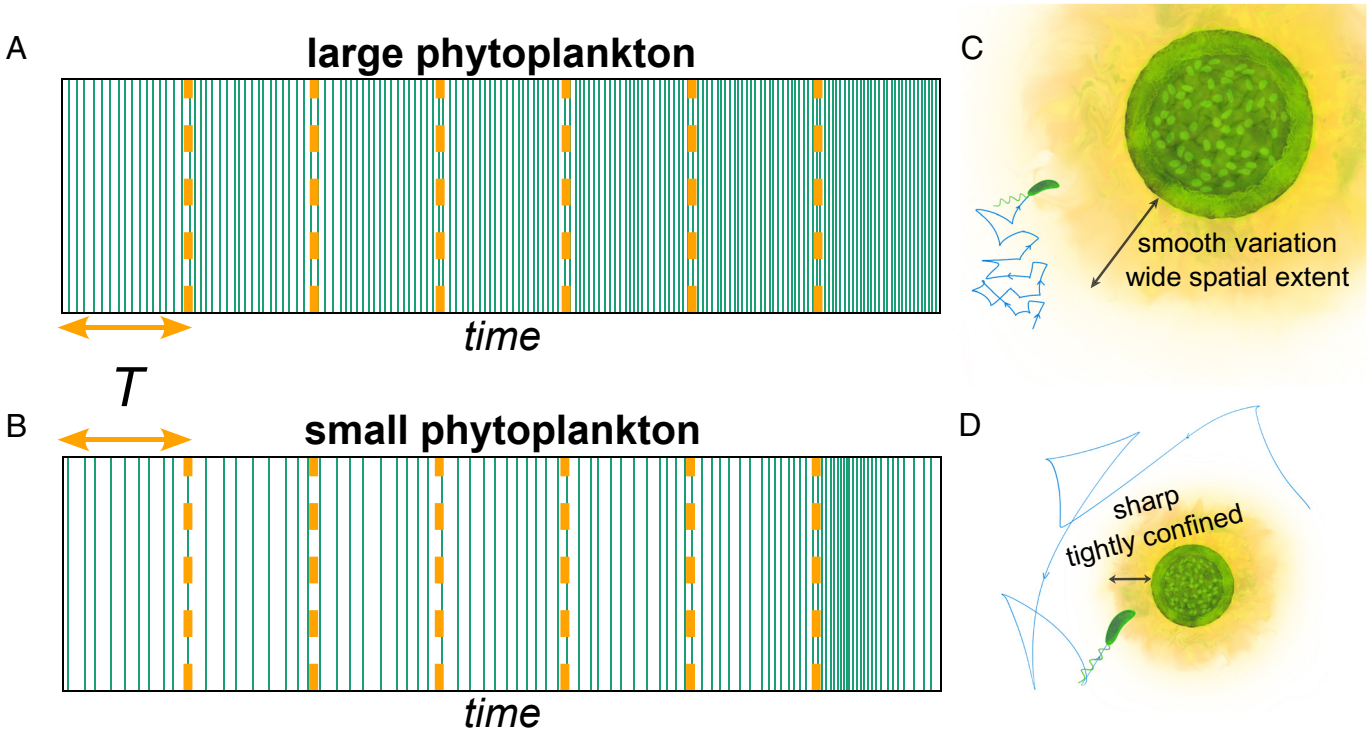

Fig. 1. Detecting chemical gradients to increase encounter rates with phytoplankton is a size-dependent challenge for bacteria. Bacteria experience concentration gradients in the form of temporal sequences of molecular adsorption events (green bars in panels *A* and *B*). Gradients are estimated by integrating the adsorption sequences over intervals of length *T*, the sensory timescale (orange broken lines). The phytoplankton size determines the lengthscale over which the gradients extend (*C* and *D*), leading to adsorption sequences with well-distinguished features for small and large sources. Large phytoplankton produce profiles with wide spatial extent: the rate of molecular adsorptions increases slowly over time and their detection is limited by molecular fluctuations (*A* and *C*). Small phytoplankton produce spatially confined profiles: the rate of molecular adsorptions increases sharply over a short time and their detection is limited by the dynamic noise arising from bacterial motion and finite temporal resolution (*B* and *D*). Timeseries were generated from simulations of Poissonian adsorption events for a bacterium moving at constant speed in the steady-state diffusive concentration field (Eq. **1**) produced by phytoplankton cells of different sizes.

dom encounters between bacteria and phytoplankton: bacteria–phytoplankton encounters are diffusive for large phytoplankton (i.e., the encounter rate scales linearly with phytoplankton size) but ballistic for small phytoplankton (i.e., the encounter rate scales quadratically with phytoplankton size) (28, 29).

Here, we explore how these limits of gradient sensing, arising from two different types of noise, one associated with inherent fluctuations and the other with the movement and sensory timescale of bacteria, determine chemotactic performance of bacteria toward phytoplankton cells. Combining the limitations on sensing with the ballistic or diffusive nature of random encounters with phytoplankton, we compute an upper bound on the chemotactic index, a dimensionless number that measures the increase in the encounter rates of bacteria with phytoplankton cells due to chemotaxis over random motility alone. Our analysis reveals an asymmetric performance landscape as a function of phytoplankton size. We find that for large phytoplankton, the chemotactic index has a weak dependence on leakage rate and bacterial phenotypes associated with motility and sensing. In stark contrast, for small phytoplankton the chemotactic index is highly sensitive to leakage rate and bacterial phenotypes. When considered in the context of encounters within marine phytoplankton communities, our findings reveal that bacteria with low swimming speed and long sensory timescales may obtain large benefits from chemotaxis in the search for small phytoplankton, whereas fast swimmers are unable to exploit chemotaxis in the search for small phytoplankton but perform consistently better in the search for larger phytoplankton.

Theoretical Model for Chemotactic Encounters

To understand how phytoplankton size affects the ability of bacteria to detect gradients, we consider an ideal bacterium whose chemotactic performance is limited only by the ability to detect a chemoattractant gradient at a distance from a phytoplankton cell. Following previous work (6, 19), we represent a phytoplankton cell as a sphere of radius R (Fig. 2*A*) that continuously exudes chemoattractant homogeneously through its surface, via either active or passive mechanisms (6). Regardless of the exudation mechanism, the chemoattractant then diffuses away from the cell. At steady state, which is reached within timescales of seconds to minutes *SI Appendix*, the concentration field around the cell is

$$C(r) = C_0 + C_S\frac{R}{r}, \qquad [1]$$

where C_0 is the background concentration of the chemoattractant far from the phytoplankton, C_S is the excess concentration of the chemoattractant at the phytoplankton cell surface (i.e., the concentration above C_0), and r is the radial distance from the center of the phytoplankton cell. In *SI Appendix*, we show that all results obtained below are also valid if bacterial

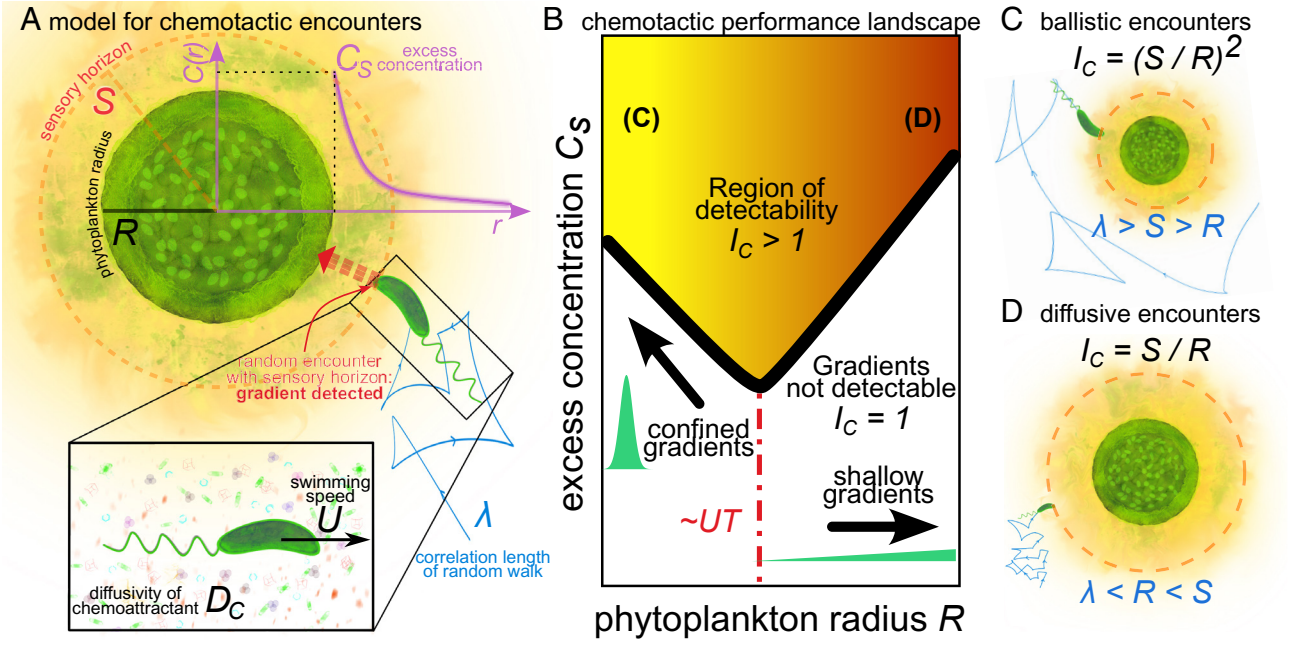

Fig. 2. Chemotactic encounters are limited by the gradients' steepness and spatial extent, and ballistic or diffusive encounters with the sensing horizon. (*A*) A phytoplankton cell of radius R produces a chemoattractant field $C(r) = C_0 + C_S R/r$ (Eq. **1**, magenta curve). C_S is the chemoattractant concentration at the phytoplankton surface in excess of the bulk background concentration C_0. Far from the cell, bacteria cannot sense the chemoattractant and thus swim in unbiased random walks, with correlation length λ. The "sensory horizon" S is the distance from the phytoplankton cell at which a perfect chemotaxer can detect the gradient and encounters its target with 100% probability (Eq. **3**). (*Inset*) Chemosensing is a molecule-counting process driven by the adsorption of individual chemoattractant molecules, which reach the bacterium via diffusion (we consider a single chemical species with diffusivity D_C) while the bacterium swims at speed U. (*B*) Depiction of the performance landscape for chemotactic searches. The phytoplankton radius R and the excess chemoattractant concentration C_S, which we treat as independent parameters both here and in Figs. 3 and 4, determine whether gradients can be successfully detected or not. For a given phytoplankton radius R, there is a minimum value of C_S for gradient detection to be possible; this set of values defines a convex boundary of detection (thick black line) which separates regions in the landscape where gradient detection is possible (the region above) or not (the region below). Below the boundary of detection, two conditions limit an organism's ability to perform chemotaxis: gradients are either too spatially confined (*Left*, Eq. **4**a) or too shallow (*Right*, Eq. **4**b). The limiting factor for detection is determined by the relationship between phytoplankton radius R and the distance traveled by a bacterium during one sensory interval, UT. In the region of detectability ($I_C > 1$) I_C is determined by the relationship between the swimming correlation length λ, the phytoplankton radius R and the sensory radius S. The size dependence of random encounters identifies two subregions within the region of detectability (here qualitatively represented by the yellow-red shading), in which the chemotactic index displays two distinct behaviors. Small phytoplankton (*C*) lead to ballistic encounters for which the chemotactic index scales quadratically with the sensory radius S, whereas for large phytoplankton (*D*) the chemotactic index scales only linearly with S due to the diffusive nature of encounters.

consumption of chemoattractant is taken into account, leading to an exponentially screened concentration field. In the absence of chemoattractants, a motile bacterium performs a random walk (30) with swimming speed U and correlation length λ (Fig. 2*A*). When chemoattractant gradients are present, the bacterium can bias its motion up the gradient, increasing its chances of encountering the phytoplankton. An exact evaluation of the encounter-enhancing effect of chemotaxis requires explicit consideration of the details of the bacterial motility and chemosensory system, which may vary significantly across species and physiological states. With the aim of seeking more general conclusions, we focus instead on computing an upper bound to the increase in encounter rates afforded by chemotaxis that will be valid for a wide variety of organisms, by considering the bacterium to be a "perfect chemotaxer." We assume that, around a phytoplankton cell, there is a sensory horizon S, which corresponds to the maximal distance at which a bacterium can reliably detect the gradient generated by the phytoplankton (Fig. 2*A*). Outside the sensory horizon no chemotaxis is possible and the bacterium moves purely by random motility, but as soon as the sensory horizon is reached, the perfect chemotaxer is able to navigate flawlessly toward the phytoplankton cell, always yielding an encounter with the phytoplankton. This concept of sensory horizon can be considered equivalent to those of capture radius, sensing range, or reaction distance often introduced in the study of predation and encounters in higher organisms (31–34). The encounter rate of the perfect chemotaxer is thus limited only by random encounters with the sensory horizon S: this simplification of the problem allows one to use existing solutions for random encounters between spherical objects (29). The problem of chemotactic encounters with the phytoplankton cell is therefore reduced to the problem of identifying the sensory horizon S, as a function of the phytoplankton radius R. Due to its idealized response, which always ensures an encounter with the phytoplankton upon gradient detection, the performance of the perfect chemotaxer is an upper limit on the performance of any real chemotactic bacterium.

The Signal-to-Noise Ratio Determines the Effectiveness of Chemotaxis

The spatial extent of the sensory horizon is defined as the distance from the phytoplankton at which bacteria can detect the gradient of chemoattractants exuded by the phytoplankton. We determine this distance in terms of the signal-to-noise ratio (SNR) associated with the bacterial measurements of the gradient, extending the approach Hein et al. (15) used to study chemotaxis toward ephemeral Gaussian pulses, by including the noise associated with the spatial confinement of the signal. In a steady concentration profile, the signal is the rate of change of concentration experienced by the bacterium over time as it swims, $|U\nabla C|$ (11, 15). The noise arises through the fluctuations in the adsorption of attractant molecules, which reach the bacterial cell surface with diffusivity D_C (Fig. 2 *A*, *Inset*) (11). In constant gradients (i.e., concentration fields varying linearly with distance from their source) the inherent noise in the gradient measurement arising from fluctuations in molecular adsorption events was derived by Mora and Wingreen (14) as $\sigma_0 = \sqrt{3C/(\pi a D_C T^3)}$. The gradient associated with the concentration field around a phytoplankton cell (Eq. **1**) is instead not constant, having a magnitude $|\nabla C(r)| = C_S R/r^2$ that increases as bacteria approach the phytoplankton and attains its maximum at the phytoplankton surface. As a step to account for this increase, we approximate the local gradient experienced by the bacterium within a single sensory window T as a linearly increasing gradient, which yields the following revised estimate of the noise *SI Appendix*,

$$\sigma_0^* = \sigma_0\sqrt{1+\frac{3}{20}\left(\frac{UT}{R+\Delta r}\right)^2}, \qquad [2]$$

where Δr is the distance from the surface of the phytoplankton cell. Eq. **2** highlights the importance of bacterial movement and phytoplankton size in the sensing process: for large phytoplankters ($R \gg UT$), at any distance Δr the correction to σ_0 is negligible; but when the phytoplankton is small compared to the distance traveled by the bacterium during the sensory interval T and the bacterium is close to the phytoplankton ($UT > R + \Delta r$), the sensing noise increases considerably. This result shows that motion in nonlinear concentration fields has the effect of a low-pass filter, which prevents bacteria from accurately measuring high-frequency variations in the concentration field, i.e., gradients tightly confined in space. Interestingly, the equation for the sensing noise highlights a tradeoff in the bacterial swimming speed: While a larger speed U increases the signal (the local gradient $|U\nabla C|$), it also increases the sensing noise in the detection of gradients generated by small phytoplankton (Eq. **2**). Higher swimming speeds may, therefore, not always be beneficial for chemotaxis to phytoplankton, in particular when phytoplankton cells are small.

While it clarifies the role of movement and size, the approximation of the gradient as locally linear, that we used to derive Eq. **2**, does not yet capture the limit of the smallest phytoplankton cells, for which the sharp increase in the gradient amplitude may be so tightly confined that it occurs within a single sensory interval T (Fig. 1 *B* and *D*). This is ecologically a very important scenario, yet we found this case to be analytically intractable. We therefore introduce, phenomenologically, a low-pass filter $f(x) = 1 - \exp(-x^{3/2})$ in the expression of the SNR, which degrades the high-frequency components of the signal ($f(x \gg 1) \sim 0$) without affecting the detection of lower frequency components ($f(x \ll 1) \sim 1$). We then define the sensory horizon S as the farthest distance from the phytoplankton cell at which the SNR is above a threshold q. S is, therefore, the solution to the equation

$$\mathrm{SNR} = \frac{|U\nabla C(S)|f(UT/S)}{\Pi\sigma_0(S)} = q, \qquad [3]$$

which we solve numerically (SI). In Eq. **3**, we introduced a constant chemotactic precision factor Π to explicitly represent noise amplification in the signal processing internal to the chemotaxis pathway (16). This choice is motivated by previous observations that in the marine bacterium *Vibrio anguillarum* the response to chemoattractant pulses was accurately described by multiplying the theoretical noise, σ_0, by a chemotactic precision factor $\Pi \approx 6$ (16). In what follows, we therefore set $\Pi = 6$. We also set $q = 1$ throughout, which equates to defining S as the distance from the phytoplankton where bacteria can detect a positive gradient with a probability of $\approx 84\%$ *SI Appendix*. While a precise numerical solution of Eq. **3** will be obtained later, an approximate calculation readily determines the boundary of detection, i.e., a curve $C_{S,\min}(R)$ in the (R, C_S) performance landscape that determines whether a phytoplankton of radius R is detectable ($C_S > C_{S,\min}(R)$) or not ($C_S < C_{S,\min}(R)$). By solving Eq. **3** in the two limit cases $S = UT$ and $S = R$, corresponding respectively to the detection being limited by

gradient confinement and gradient steepness, and with the additional approximation $C_0 = 0$, we obtain two curves *SI Appendix*

$$C_{S,\min}^{\text{left}} \approx 34.4 \frac{U}{aD_C R}, \qquad (S = UT) \qquad \textbf{[4a]}$$

$$C_{S,\min}^{\text{right}} \approx 34.4 \frac{R^2}{aD_C U^2 T^3}, \qquad (S = R) \qquad \textbf{[4b]}$$

which define a convex region in the space of phytoplankton phenotypes R and C_S (Fig. 2*B*), that we call the region of detectability, where bacteria can detect the gradients produced by phytoplankton cells.

When gradient detection is possible, the performance of a bacterium's search for a phytoplankton is limited by its random encounters with the sensory horizon, since no chemotaxis is possible outside the sensory horizon. For perfect chemotaxis, reaching the sensory horizon S ensures that the bacterium will eventually reach the phytoplankton cell: The problem of chemotactic encounters with the phytoplankton cell thus simplifies to the problem of random encounters with the sensory horizon. We can then quantify the maximum possible performance of a chemotactic search through the chemotactic index, I_C, which we define as the ratio between the rate of random encounters with the sensory horizon S and the rate of random encounters with the phytoplankton cell of radius R, as

$$I_C = \Gamma(S)/\Gamma(R). \qquad \textbf{[5]}$$

$\Gamma(x)$ is the encounter kernel that quantifies the random encounters of the bacterium with a target of radius x and represents the amount of volume swept per unit time by the motion of the bacterium relative to the phytoplankton (28, 29, 32). For simplicity, we only consider nondestructive encounters (35), in which the phytoplankton and chemical gradients remain unaffected by the encounter event. Moreover, we ignore stages of interaction successive to the encounter with the sensory horizon, after which the bacterium might, for example, reside in the proximity of the phytoplankton for prolonged times (20) and experience multiple successive encounters with the same phytoplankton. Chemosensing is successful and increases encounters when the bacterium can detect a gradient at a distance from the phytoplankton cell, that is when a sensory horizon $S > R$ exists; in this case, the chemotactic index will be $I_C > 1$. When a sensory horizon $S > R$ does not exist, bacteria cannot detect gradients at a distance from the phytoplankton cell, so chemotaxis cannot enhance encounter rates and therefore $I_C = 1$ (we ignore possible scenarios where chemotaxis is detrimental to encounters, leading to $I_C < 1$). Within the region of detectability ($I_C > 1$, Fig. 2*B*), I_C is determined by the relationship between the correlation length of the bacterial random walk, λ, the phytoplankton radius, R, and the sensory horizon, S (*SI Appendix*, Eq. **S44**). In particular, the encounters with small phytoplankton cells ($\lambda > S > R$) have a ballistic nature ($\Gamma \sim R^2$) (36) and result in a quadratic scaling of the chemotactic index with the sensory horizon, $I_C = S^2/R^2$ (Fig. 2C). For large phytoplankton cells ($\lambda < R < S$) encounters have a diffusive nature ($\Gamma \sim R$) (37, 38) and the chemotactic index scales only linearly with the sensory horizon, $I_C = S/R$ (Fig. 2*D*).

We note that our definition of the chemotactic index is analogous to that used in the in situ chemotaxis assay (ISCA). The ISCA is a microfluidic assay for deployment in aqueous environments. It measures the strength of bacterial chemotaxis to a given compound in situ by comparing the number of bacteria that accumulate, after a given deployment time of typically 1 h, in a well filled with that compound, to the number of bacteria found in a negative control well devoid of chemoattractants (1, 39, 40). Our results may, therefore, be interpreted as providing an upper bound on the chemotactic index obtained in ISCA experiments with inlets of different sizes containing chemoattractants in different concentrations. We next solve Eq. **3** numerically for S and use the solution to compute I_C according to Eq. **5** and thus quantify the chemotactic performance as a function of bacterial and phytoplankton phenotypes.

Asymmetry of Chemotactic Performance

We find that chemotaxis toward small phytoplankton cells can be risky but highly rewarding. We illustrate this by applying our model to a typical motile marine bacterium with radius $a = 0.5$ μm, swimming speed $U = 50$ μm/s and sensory timescale $T = 100$ ms, that is chemotactic toward a low-molecular-weight compound with diffusivity $D_C = 500$ μm^2/s (Fig. 3). We assume the background concentration of the compound (C_0 in Eq. **1**) to be 1 nM, typical of oligotrophic ocean waters (13) (calculations with different background concentrations are shown in *SI Appendix*, Fig. S6). Using our model, we quantified the chemotactic performance landscape by computing the chemotactic index as a function of the phytoplankton radius R and the excess concentration C_S (which is proportional to the phytoplankton leakage rate). We stress that, in the analysis below, C_S and R are free parameters; later, we will include the physiological constraints the cell size imposes on the excess concentration. The performance landscape exhibits a convex, V-like, shape, with its apex around $R \approx UT$, as predicted by the approximate Eq. **4**, and shows a marked asymmetry between small and large phytoplankton (Fig. 3*A*). Specifically, the chemotactic index has a much sharper dependency on C_S when the phytoplankton radius R is small ($R < 2$ μm in this example), especially close to the boundary of detection ($I_C = 1$) (Fig. 3*B*). This indicates that even modest variations in the excess concentration C_S leaked by a small phytoplankton can have large impacts on the performance of bacterial chemotaxis. In the example, while bacteria will not be able to sense ($I_C = 1$) an attractant gradient from a 1 μm phytoplankton creating an excess concentration of $C_S = 10$ nM, a moderately higher value $C_S = 30$ nM yields a high chemotactic index $I_C = 10$. As C_S is further increased, the dependency of I_C on C_S becomes weaker. For larger phytoplankton cells, the increase in performance is more gradual: above the boundary of detection ($I_C = 1$), I_C grows slowly with increasing C_S. Looking across phytoplankton radii R, for small values of the excess concentration C_S an increase in R leads first to a sharp increase in chemotactic index and then a gradual decrease toward $I_C = 1$ when R exceeds an optimal value (Fig. 3*C*).

The behavior of the chemotactic index close to the boundary of detection ($I_C = 1$) reveals the origin of the asymmetry in the chemotactic performance landscape. For chemotaxis toward large phytoplankton (right boundary), gradient detection is limited by gradient steepness. If the excess concentration of chemoattractant around the phytoplankton is just sufficient to allow gradient detection, the sensory horizon will only be marginally bigger than the size of the phytoplankton, $S = R(1 + \varepsilon)$ (where $\varepsilon \ll 1$), because the gradients in the concentration profile in Eq. **1** are steepest near the phytoplankton. Since encounters with large targets are diffusive, the encounter rate is proportional to target size, yielding $I_C \sim S/R \sim 1 + \varepsilon$: the chemotactic index increases

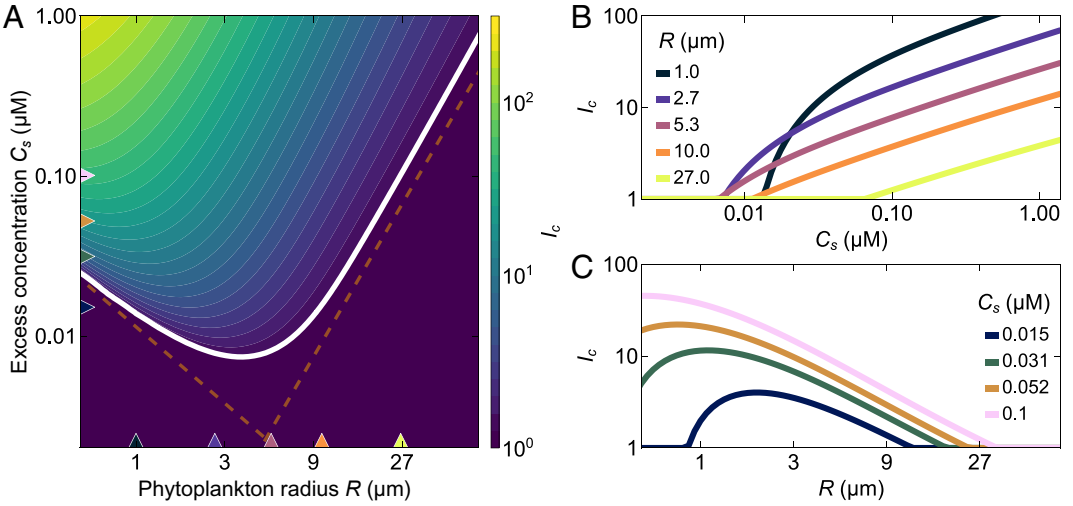

Fig. 3. The stakes are high for encounters with small phytoplankton—the chemotactic index is largest for small phytoplankton, but it drops sharply when gradient detection fails. (*A*) Performance (I_C) landscape for a bacterium using chemotaxis to drive encounters with spherical targets of different radii (R) and chemoattractant concentrations (C_S) calculated using Eqs. **3** and **5** (see also *SI Appendix*, Eq. **S44**). The thick white line defines the boundary of detection, separating the region where gradients are detectable and chemotaxis is beneficial to encounters ($I_C > 1$) from the region where gradients are too shallow or too spatially confined to be detected ($I_C = 1$). Broken orange lines are the approximate predictions for the minimum value of C_S at which detection is possible (Eq. **4**). (*B*) Vertical transects from panel *A* for fixed values of the target radius R (corresponding to the upward-pointing triangles). In chemotaxis toward small targets, a slight variation in the chemoattractant concentration can make the difference between a highly successful search ($I_C \approx 10$) or a failure ($I_C = 1$), whereas for larger targets the dependency of I_C on the chemoattractant concentration is more gradual. (*C*) Horizontal transects from panel *A* for fixed values of the chemoattractant concentration C_S (corresponding to the right-pointing triangles). For weak sources, an increase in size R produces initially large enhancements in chemotactic performance, with diminishing returns upon further enlargement. As the source gets stronger, the increase in performance for chemotaxis toward small targets becomes disproportionately larger; larger sources also become detectable although offering modest performance improvements over random searches. A script to generate an interactive dashboard for the rapid evaluation of the I_C landscape is available from GitHub (see Movie S1 for a demo).

smoothly as the boundary of detection is crossed. By contrast, for small phytoplankton (left boundary), gradient detection is limited by the gradient's spatial extent. The minimal sensing horizon that can be detected is therefore on the order of the distance traveled by the bacterium in a single sensory interval, $S \sim UT$. Since encounters with small cells are ballistic, the encounter rate is proportional to the square of the target size, and thus $I_C \sim (S/R)^2 \sim (UT/R)^2$: the chemotactic index exhibits a large jump from 1 to $(UT/R)^2$ as the boundary is crossed. For example, in Fig. 3, we have $UT = 5$ μm, which implies a jump of the order $(UT/R)^2 \sim 25$ for a small phytoplankton cell with $R = 1$ μm, which captures the order of magnitude of the jump observed in Fig. 3*C* (green line). We next show that this asymmetry of the performance landscape is robust to changes in the key parameters.

Dependence of Chemotactic Performance on Physical Parameters

Variations in the swimming speed U, the sensory timescale T and the chemoattractant diffusivity D_C, determine the performance of chemotaxis for a given phytoplankton radius and excess concentration, but do not affect the fundamental structure of the performance landscape (Fig. 4). This can be seen by comparing the landscapes obtained through the variations in individual parameters against the reference landscape computed in Fig. 3, where we used $U = 50$ μm/s, $T = 100$ ms, and $D_C = 500$ μm^2/s. A reduction in the sensory timescale T from 100 to 50 ms [two values on the low end of the estimates for bacterial sensory timescales (11, 19, 41–43)] decreases the ability of bacteria to detect gradients from large phytoplankton cells and reduces the overall performance of chemotaxis (Fig. 4*A*; *SI Appendix*, Figs. S7*A* and S8*D*). A smaller value of T is associated with a larger sensing noise ($\propto T^{-3/2}$) but with a smaller dynamic noise because the measurement frequency is increased. The position of the left boundary of detection is unaffected by the variation in T (Eq. **4**a) but the right boundary is shifted toward larger values of C_S as T increases (Eq. **4**b). An increase in the swimming speed U from 50 to 100 μms [respectively a moderate and a large value for the average swimming speed of marine bacteria (23, 44)] improves the performance of chemotaxis within the region of detectability (since the raw signal $|U\nabla C|$ increases), but the region of detectability itself is shifted toward larger values of the phytoplankton radius: as U increases, higher C_S is required to detect small phytoplankton (Eq. **4**a) but lower C_S is required to detect large phytoplankton (Eq. **4**b). This result highlights that an increased swimming speed results in a tradeoff between degraded spatial resolution, due to the lower frequency of measurements, and improved sensitivity (Fig. 4*B*; *SI Appendix*, Figs. S7*B* and S8*E*). A surprising consequence is that lower swimming speeds may improve the performance of chemotactic searches toward small phytoplankton cells. An increase in the diffusivity of the chemoattractant D_C from 500 to 1,000 μm^2/s (values which are representative respectively of sugars (45), and DMSP (46) or amino acids (47)) enhances the SNR (sensing noise $\propto D_C^{-1/2}$) without affecting spatial resolution, and thus shifts the region of detectability toward lower C_S values (Fig. 4*C*; *SI Appendix*, Figs. S7*C* and S8*F*), as also described by the $1/D_C$ dependency of the two boundaries (Eq. **4**). In summary, we have shown that bacterial chemotactic searches for phytoplankton cells are characterized by a fundamental asymmetry in the performance, which does not depend on the specific values of the parameters involved in the search: the performance of chemotaxis toward large phytoplankton varies smoothly with variations in leakage rate and other parameters, while the performance of chemotaxis toward small phytoplankton is highly sensitive to variations in the search parameters and may exhibit sudden jumps between high-gain and no gain at all ($I_C = 1$). This suggests an interpretation

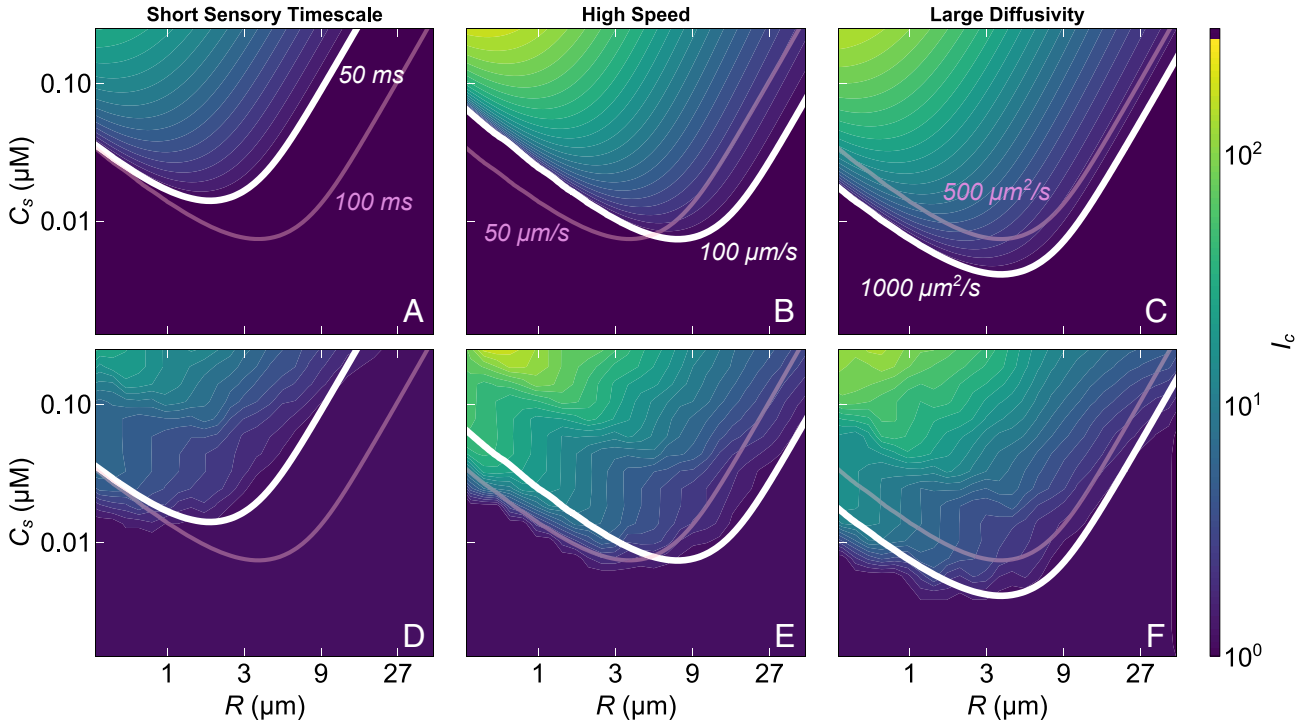

Fig. 4. Bacterial phenotypes and chemoattractant diffusivity control the chemotactic index but do not alter the high-stakes nature of encounters with small phytoplankton. Performance landscapes of different chemotactic strategies obtained from theoretical (*A–C*) and computational (*D–F*) models. In all the panels, the pink curve is the detection boundary for a reference system with swimming speed $U = 50$ μm/s, sensory timescale $T = 100$ ms, and chemoattractant diffusivity $D_C = 500$ μm/s^2 (same as in Fig. 3*A*). (A) Reduction in sensory timescale T from 100 ms to 50 ms. (*B*) Increase in swimming speed from 50 μm/s to 100 μm/s. (*C*) Increase in chemoattractant diffusivity from 500 μm^2/s to 1,000 μm^2/s. (*D–F*) Theoretically predicted features of bacterial chemotactic performance are reproduced by a minimal model of an ideal sensor based on the Kolmogorov–Smirnov test. In panels *D–F*, the white line is the detection boundary from the theoretical prediction of panels *A–C*, respectively; the heatmap represents values of the chemotactic index obtained from numerical simulations of the ideal sensor (linearly interpolated). Despite small quantitative differences in the estimated I_C values, arising from the distinct signal processing mechanism and the finite spatial resolution of numerical simulations, the features of the performance landscape (shape and asymmetry) are clearly conserved.

of chemotaxis to small phytoplankton cells as a high-stakes adaptation.

An Ideal Sensor Model

To demonstrate that our conclusions are not the result of specific model choices, we further develop a more general framework based on a minimal numerical model of an ideal sensor (Fig. 4 *D–F*). This ideal sensor is defined as a sphere moving at constant speed U toward a phytoplankton cell surrounded by a chemoattractant field $C(r)$. As it moves, the ideal sensor registers all the adsorption events of chemoattractant molecules, occurring as Poisson events with instantaneous rate $4\pi D_C a C(r)$, where r is the instantaneous distance of the sensor from the center of the phytoplankton. After a time interval T, all registered events are processed and a new acquisition starts. For signal processing, the sensor performs a one-sided Kolmogorov–Smirnov test (48) comparing the distribution of the waiting times between successive adsorption events recorded in the first and the second half of the acquisition interval T. If the cumulative distribution function is larger in the second half of the interval than in the first half (with P-value $P < 0.05$), then the sensor has detected a positive gradient. Averaging the successful gradient detections over an ensemble ($N = 1{,}000$) of such ideal sensors provides an estimate of the sensory distance S, defined as the largest distance r, where at least a fraction f of the sensors has detected a gradient. The estimates of S can then be used to evaluate the chemotactic index I_C as we have done for the bacterial model (Eq. **5**). Remarkably, we find that with a high consensus threshold ($f = 0.99$), the ideal sensor model provides close agreement with our theoretical calculations, both in terms of the V-shape of the detectability region and of the predicted I_C values (Fig. 4 *D–F*). One discrepancy is the exact location of the left boundary of the detectability region, which reflects the sensitivity of the chemotactic index to the details of the signal processing, i.e., to the way high-frequency signals are degraded. In Eq. **3**, we represented the signal degradation through the phenomenological low-pass filter $f(x)$; the Kolmogorov–Smirnov sensor still shows low-pass characteristics for small phytoplankton but the filtering function is different (for a detailed discussion of this minimal model and the simulation procedure, see *SI Appendix* and *SI Appendix*, Fig. S9). This close agreement highlights the generality of our findings, since they are recapitulated by an ideal sensor lacking many of the specific search characteristics of a chemotactic bacterium. We next explore the ecological consequences of the asymmetry in the performance of bacterial chemotaxis toward phytoplankton, by taking into account physiologically realistic values of the excess concentration and using the resulting chemotactic indices to estimate typical search times in phytoplankton communities.

Chemotactic Encounters in Marine Phytoplankton Communities

The physiological range of exudation rates for healthy phytoplankton cells spans a region crossing the boundary of chemotactic detection ($I_C = 1$, Fig. 5*A*). Up to now, we have considered the excess concentration C_S as a free parameter that could take on

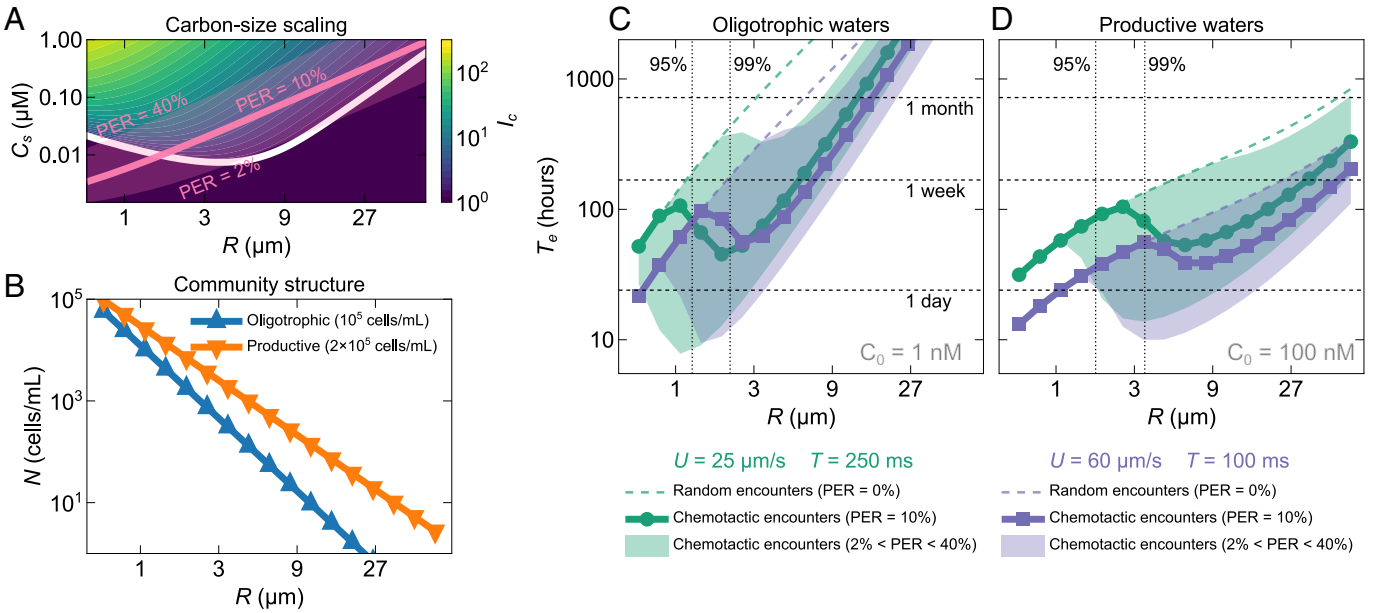

Fig. 5. The asymmetric performance of bacterial chemotaxis toward phytoplankton cells may promote a diversity of search phenotypes. (*A*) Characteristic values of size and released chemoattractant for phytoplankton cells are constrained by carbon-size scaling laws (pink areas). When overlaid on the performance landscape of a bacterium (same as in Fig. 3*A*), the physiological range of exudation rates lies across the boundary of detection. The thick pink line corresponds to phytoplankton cells with a percent extracellular release (PER) of 10%, the shaded pink band represents variations in the PER between 2% (lower limit) and 50% (upper limit). (*B*) Marine phytoplankton communities are dominated by small cells. The size structure follows a power-law distribution, where the abundance N decreases with increasing size R as $N(R) \propto R^{-3\alpha}$. The allometric exponent is larger in oligotrophic waters ($\alpha = 1.0$) than in more productive waters ($\alpha = 0.75$). For the oligotrophic community we assume a total abundance of 1e5 cells/mL, and 2e5 cells/mL for the productive community. (*C* and *D*) Comparison of average search times between random motility and chemotaxis. Carbon-size scaling, phytoplankton community structure, and chemotactic index jointly define the average search time (T_e) (Eq. **6**) an individual bacterium requires to encounter a phytoplankton cell using chemotaxis. The thin broken lines represent the search times in the absence of chemotaxis ($I_C = 1$). The thick lines with markers indicate search times for phytoplankton cells with PER of 10% (corresponding to the thick pink line in panel *A*), and the shaded bands represent variations in PER between 2% and 40% (matching the pink shaded band in panel *A*). The two curves correspond to distinct bacterial phenotypes: in green with circle markers, a bacterium with low speed and long sensory timescale; in violet with square markers, a bacterium with high swimming speed and short sensory timescale. The vertical dotted lines mark the radii corresponding to the 95th and 99th percentiles of the phytoplankton community abundance. A script to generate an interactive dashboard for the rapid evaluation of search times is available from GitHub (see Movie S2 for a demo).

a wide range of values. The physiology of marine phytoplankton, however, imposes a coupling between cell size R and excess concentration C_S so that for a phytoplankton of a given size, a narrower range of C_S values is most typical. Empirical carbon-size scaling laws predict that the carbon content of a phytoplankton cell scales with cell radius as $\sim R^{2.28}$ (49). The percent extracellular release (PER), defined as the dissolved fraction of the total primary production (4, 50), then determines the rate at which the phytoplankton cell leaks carbon to the environment, in the form of dissolved organic matter (6, 19) (see *SI Appendix* for details). PER values are of the order of 10% (i.e., 10% of the total primary production is exuded instead of being metabolized for growth), but can range from 2% up to 40%, highlighting the strong dependence of the release rate on physiological and environmental conditions (51). Higher PER values may be correlated with higher stress levels of the phytoplankton, resulting in the inability to store or metabolize carbon. For any given phytoplankton radius R, we thus obtain a range of exudation rates (corresponding to a range of PER values) which determine the excess concentration C_S at the surface of the phytoplankton cell (*SI Appendix*, Eqs. **S1**–**S7**). Overlaying this range of ecologically relevant values onto the chemotactic performance landscape (Fig. 5*A*) reveals that chemotaxis might increase encounters across the entire phytoplankton size spectrum. Bacterial detection of the gradients generated by the smallest phytoplankton cells ($R < 3$ μm) may only be possible at high PER levels, whereas at low PER levels the gradients may be too tightly confined in space for bacteria to detect them.

The steeply decreasing size structure of marine phytoplankton communities favors encounters of bacteria with small phytoplankton cells. The average search time T_e required by one bacterium to encounter a phytoplankton cell is *SI Appendix*

$$T_e = \frac{1}{I_C(R)\Gamma(R)N(R)}, \qquad [6]$$

where $N(R)$ is the concentration of phytoplankton of radius R and $\Gamma(R)$ is the random encounter kernel between bacteria and phytoplankton of size R. Marine phytoplankton communities have size structures that usually follow a power-law size-abundance relationship of the form $N(R) \propto R^{-3\alpha}$, where the allometric exponent α takes values between $\alpha \approx 1.0$ in oligotrophic waters and $\alpha \approx 0.75$ in productive waters (18). Phytoplankton cells with small radii are, therefore, vastly more abundant than those with large radii, particularly so in oligotrophic environments where large phytoplankton are very rare (Fig. 5*B*). Moreover, we consider an overall larger cell abundance in productive waters (a total of 2e5 cells/mL between 0.5 and 70 μm in radius) with respect to oligotrophic waters (a total of 1e5 cells/mL between 0.5 and 70 μm in radius) (18). Larger cell abundances are also reflected in higher background chemoattractant concentrations, for which we assume $C_0 = 1$ nM in oligotrophic waters and $C_0 = 100$ nM in productive waters (13). We first note that, in the absence of chemotaxis, the steep size structure of phytoplankton communities alone results in bacterial search times that are much shorter for small

phytoplankton than for larger ones (broken lines in Fig. 5 *C* and *D*). In both environments, a faster bacterium with $U = 60$ μm/s (thin violet broken lines in Fig. 5 *C* and *D*) will experience shorter search times across the entire size spectrum since faster swimming always increases the rate of random encounters. We now show that, when chemotaxis is taken into account, the asymmetric performance landscape of bacterial chemotaxis further raises the stakes for bacterial encounters with phytoplankton at the low end of the phytoplankton size spectrum.

Chemotaxis can markedly reduce search times for phytoplankton in the sub-5 μm size range, but different bacterial phenotypes display substantial performance differences in the low end of the phytoplankton size spectrum (Fig. 5 *C* and *D*). The decrease in search time afforded by chemotaxis over the whole range of phytoplankton PER values considered is shown as a shaded band in Fig. 5 *C* and *D*, with the thick marker-decorated line representing PER = 10%. In oligotrophic waters, slower bacteria ($U = 25$ μm/s) with a longer sensory timescale ($T = 250$ ms) decrease their search times for the smallest phytoplankton by almost a factor 10 compared to random motility, whereas faster bacteria ($U = 60$ μm/s) with a shorter sensory timescale ($T = 100$ ms) cannot benefit at all from chemotaxis at this low-end of the phytoplankton size spectrum and may be outperformed by the slow swimmers when the phytoplankton PER is high (Fig. 5*C*). While the major difference in the I_C values between the two strategies just considered is limited to phytoplankton in the micrometer range, this region of the size spectrum encloses the vast majority of the phytoplankton: in both environments, the 95th percentile of the population (dotted vertical lines in Fig. 5 *C* and *D*) is below the 2 μm radius. We also note that the boost in chemotactic performance toward small cells occurs only at high PER values, whereas no gain is obtained at intermediate or low PER values. This indicates that chemotaxis toward small phytoplankton may be primarily beneficial when phytoplankton cells are very leaky, as occurs, for example, in the late stages of a bloom or for damaged or senescent individuals (4) (see also *SI Appendix* for discussion on the effect of chemoattractant diffusivity). In contrast, for larger (>2 μm) phytoplankton, both phenotypes can benefit from chemotaxis also at lower PER values; while the resulting search times are comparable, the fast swimmers display shorter search times. In productive waters, where large cells are more abundant and the background concentration of chemoattractants is higher, neither of the two bacterial phenotypes is able to use chemotaxis to reduce search times for phytoplankton cells smaller than ∼2 μm (Fig. 5*D*). Here, the faster bacteria outperform the slower ones in the search for phytoplankton over the entire size spectrum.

To further characterize the impact of chemotaxis on encounters within phytoplankton communities, we integrate the search times (Fig. 5 *C* and *D*) over the phytoplankton size spectrum Over the course of 1 d, a typical bacterial lifetime (52), an individual slow-swimming bacterium in oligotrophic environments will experience, on average, between 1 random (PER = 0) and 13 chemotactic (PER = 40%) encounters, and a faster bacterium will similarly experience 3 random (PER = 0) to 12 chemotactic (PER = 40%) encounters. When integrated across the phytoplankton size spectrum, the superior chemotactic performance of slow swimmers toward picophytoplankton thus offsets the random encounter advantage of fast swimmers, supporting the idea that the two search phenotypes may coexist in oligotrophic oceans. In productive waters, a slow swimmer would experience 3 to 14 encounters per day, while a fast swimmer would range between 8 and 21 encounters per day. We can thus conclude that chemotaxis can enhance bacteria–phytoplankton encounters up to 10-fold compared to random motility. To obtain the total number of encounters occurring in a given volume of seawater, these numbers must be multiplied by the concentration of heterotrophic bacteria (1e5 cells/mL in oligotrophic waters and 1e6 cells/mL in productive waters, of which we consider only 10% to be motile) (44, 53). The results predict that there are up to 8e4 bacteria–phytoplankton chemotactic encounters occurring every day in a milliliter of oligotrophic waters, and up to 1.7e6 in a milliliter of productive waters (*SI Appendix*, Fig. S10). Moreover, if we assume the individual encounters to be Poissonian events *SI Appendix*, the search times will follow an exponential distribution, so that if the average search time is T_e, half of the encounters will occur in less than $0.7T_e$, and 10% of them will occur in less than $0.1T_e$.

Discussion

The differences in the chemotactic performance of two representative bacterial phenotypes showcased in Fig. 5 highlight how the tradeoff between higher swimming speed and sensing noise in chemotaxis toward small phytoplankton (Eq. **2**) may only be relevant under certain environmental conditions. Low swimming speeds and long sensory timescales may be considered a high-risk adaptation that provides very high gains: Although bacteria with such phenotypes are otherwise outperformed by faster swimmers, they can have superior performance in the search for very leaky picophytoplankton, which may constitute the most favorable niche in conditions where nutrients and large phytoplankton are scarce. Higher swimming speeds, which provide a higher baseline rate of random encounters at the cost of reduced chemotactic performance in the low end of the phytoplankton size spectrum, are instead a low-risk adaptation, offering robust gains across a wider range of conditions. We propose that this asymmetry can be a promoter of coexistence between diverse search phenotypes in bacterial populations.

The chemotactic encounter problem can be seen as an evolutionary game where search time is one of the factors influencing the fitness of bacteria. It is important to keep in mind, however, that the encounter with the sensory horizon is only the first step of a multistage interaction process and that fitness is ultimately determined by the ability to grow and reproduce ("growth return"). A more complete ecoevolutionary picture would require simultaneous knowledge of the search time and the growth return associated with phytoplankton cells of different sizes. In this respect, chemotaxis is expected to not only reduce search times but also improve growth returns by allowing bacteria to remain near a phytoplankton cell, where concentrations of dissolved organic matter are higher (54). Indeed, Raina et al. (20) have shown that *M. adhaerens* can use chemotaxis to increase both nitrogen uptake from *Synechococcus* cells and encounter rates with their phycosphere. Generally, it can be expected that larger phytoplankton, while offering less drastic enhancements in search times through chemotaxis, provide larger growth returns, yet a quantitative consideration of the growth return should also include estimates of the energy expenditure associated with motility (which increases quadratically with swimming speed) and chemotaxis (55, 56), and the mortality cost associated with predation, which may increase with swimming speed or as a result of extended residence times in nutrient-rich regions (57, 58). Future research in this direction may consider more sophisticated encounter models, able to account for example for hovering, reversible and irreversible attachment, spatial correlations in dense algal blooms, and even destructive

effects on the organisms, such as phytoplankton cells being killed by bacteria (32, 35, 59, 60).

Our results show that the limits of the chemotactic search for small phytoplankton cells are sensitive to the details of motility and sensing. Almost 40 y ago, Jackson hypothesized that the gradients around small cells could not be sensed by a swimming bacterium (19). However, recent observations, such as the aforementioned *M. adhaerens*–*Synechococcus* interaction (20) or the investigation of the chemotactic response of marine heterotrophic bacteria to the exudates of virus-infected *Synechococcus* extending to distances larger than 100 μm (61), indicate that this limit is not universal. Our results provide the foundation that confirms that micrometer-sized targets are generally detectable by chemotactic bacteria and that chemotaxis can significantly reduce the search time for such small cells, under certain conditions (Fig. 5). Our findings also show that the exact position of the detection boundary is sensitive to the search parameters, including bacterial swimming speed, sensory timescale and chemotactic sensitivity, phytoplankton size and leakage rate, and molecular diffusivity of the chemoattractant (Fig. 4). Consequently, chemotaxis toward phytoplankton may be more pervasive than previously thought (62), yet questions related to its operational limits or its quantitative benefit for bacterial growth may need to be investigated for each specific system.

More work is needed to evaluate how close to the predicted idealized chemotactic performance bacteria can operate. Agent-based simulations of bacterial chemotaxis toward leaky phytoplankton cells could help to establish the distance to the idealized limit as a function of bacterial phenotypes and chemotactic strategy (i.e., the behavioral response elicited after the detection of a gradient). It is known that different strategies exist (21, 63–66), but the full extent of their diversity and their performance in the context of chemotaxis toward phytoplankton is unclear. Our work indicates that optimal strategies may depend on the phytoplankton cell size—strategies that work well for large cells will likely underperform for small ones and vice versa. Moreover, experiments designed to assess how far from a phytoplankton cell chemoattractants can be detected by bacteria could aid in providing a stronger connection between the mathematical notion of a sensory horizon (Fig. 2) and the empirically grounded concept of the phycosphere (6, 67, 68), the biochemically rich microenvironment which surrounds individual phytoplankton cells.

Beyond bacterial chemotaxis, other forms of taxis and kinesis are widespread in nature, from spatial chemotaxis in leukocytes (69), through olfactory navigation in insects (70) to visual feeding in fishes (71). Common features of natural search strategies have been identified (72), and the predictions of generalized frameworks for sensory searches (e.g., the effect of the search on the stability of antagonistic and mutualistic interactions), depend strongly on the size of the sensory region (73). Our results show that the transition from ballistic to diffusive encounters with the sensory region and the size-dependent limitations on signal perception together impose tradeoffs that determine an asymmetry in the performance of bacterial chemotaxis toward phytoplankton. Due to their fundamental nature, similar tradeoffs may apply to a broader class of systems having different sensory mechanisms. Investigating mathematical descriptions of the SNR associated with different sensory systems (74) in terms of the search parameters, particularly movement speed, reaction time, and target size, may provide valuable insights into the efficiency and limitations of other natural search strategies.

Our analysis is based on several simplifying assumptions. Phytoplankton exudates typically vary in composition and abundance as a function of the organism's identity, physiological conditions, and life stage (4, 6, 51). We only model chemoattractants through their diffusivity, but different bacteria are attracted to distinct compounds with varying sensitivity (1, 75), many chemoattractants can drive behavioral and metabolic shifts in bacteria (76–79), and how the co-occurrence of multiple compounds may impact chemotactic responses is still mostly not understood (40, 80). Turbulence in the water column can transport the microorganisms and deform the concentration profiles around phytoplankton cells, enhancing or degrading chemotactic performance in ways that strongly depend on turbulent intensity, phytoplankton size, and bacterial speed (81–84), although at the low intensities typical of the ocean (85), we may expect its contribution to mostly enhance encounters. Temporal fluctuations, from daily to seasonal cycles, drive variations in cell abundances (86, 87), rescaling the search times proportionally, as well as in leakage rates (88) and bulk concentrations of chemicals (89). All these factors and others, such as predation (57), sinking (90, 91) and viral infections (92, 93), contribute to shaping the microscale interaction landscape of the ocean.

Conclusions

Using idealized models of phytoplankton leakage and bacterial chemotaxis, we calculated upper bounds on the enhancement in bacteria–phytoplankton encounters driven by chemotaxis over random motility alone and studied how the enhancement depends on the size of the phytoplankton and on bacterial phenotypes. We found that bacterial chemotaxis offers low-risk/low-gain performance in the search for large phytoplankton but high-risk/high-gain performance in the search for small phytoplankton. This fundamental tradeoff arises from chemotactic encounters being limited by different mechanisms at the two ends of the phytoplankton size spectrum. For large phytoplankton, the limitation stems from the small steepness of the gradients and the diffusive nature of bacterial motility, which leads to moderate but consistent reductions in search times due to chemotaxis. By contrast, for small phytoplankton, the limitation stems from the small spatial extent of the gradients and the ballistic motility of bacteria, which leads to large yet less reliable reductions in search times due to chemotaxis. Furthermore, we found that searching for small phytoplankton is more efficient when bacteria swim more slowly and integrate the gradients over longer sensory timescales. Overall, our results suggest that the high-stakes nature of encounters with small phytoplankton is a fundamental feature of chemotactic searches that may drive a diversity of size-sensitive chemotactic strategies among marine bacteria.

Materials and Methods

All the data shown in this work has been generated through custom Julia (version 1.10) code, which is available on GitHub: (94). Project codes and data were managed with DrWatson.jl (95). Numerical solution of the equations for the evaluation of the sensory horizon S was performed with the `OrderO` method (96) implemented in the Roots.jl library. Simulations for the Kolmogorov–Smirnov model sensor made use of Distributions.jl (97) and HypothesisTests.jl. Figures were realized with Makie.jl (98) and Inkscape. Interactive dashboards were realized with Makie.jl (98).

Data, Materials, and Software Availability. Custom Julia code used to generate data has been deposited in GitHub (94).

ACKNOWLEDGMENTS. We thank Johannes Keegstra and Thomas Kiørboe for discussions. We gratefully acknowledge funding from the European Union's Horizon 2020 research and innovation program under Marie Skłodowska-Curie Grant No. 955910 to R.F.; a Gordon and Betty Moore Foundation Symbiosis in Aquatic Systems grant (Grant 9351) to D.R.B.; the "Agence Nationale de la Recherche" under Grant ANR-22-CPJ2-0015-01 to F.J.P.; a Gordon and Betty Moore Foundation Symbiosis in Aquatic Systems Initiative Investigator Award (GBMF9197), the Simons Foundation through the Principles of Microbial Ecosystems collaboration (Grant 542395FY22), Swiss NSF grant 205321_207488, Swiss NSF Sinergia grant CRSII5-186422, and the Swiss NSF, National Centre of Competence in Research Microbiomes (No. 51NF40_180575) to R.S.; a Swiss NSF Ambizione grant no. PZ00P2_202188 to J.S. We also gratefully acknowledge ETH Zürich (Euler cluster) for providing computational resources.

Author affiliations: [a]Institute of Environmental Engineering, Department of Civil, Environmental and Geomatic Engineering, ETH Zürich, Zürich 8093, Switzerland; [b]School of Mathematics and Statistics, The University of Melbourne, Parkville, VIC 3010, Australia; and [c]Institut de Physique de Rennes, University of Rennes, CNRS, Rennes F-35000, France

1. J. B. Raina *et al*., Chemotaxis shapes the microscale organization of the ocean's microbiome. *Nature* **605**, 132–138 (2022).
2. F. Azam, Microbial control of oceanic carbon flux: The plot thickens. *Science* **280**, 694–696 (1998).
3. J. B. Raina, V. Fernandez, B. Lambert, R. Stocker, J. R. Seymour, The role of microbial motility and chemotaxis in symbiosis. *Nat. Rev. Microbiol.* **17**, 284–294 (2019).
4. D. C. Thornton, Dissolved organic matter (DOM) release by phytoplankton in the contemporary and future ocean. *Eur. J. Phycol.* **49**, 20–46 (2014).
5. S. Smriga, V. I. Fernandez, J. G. Mitchell, R. Stocker, Chemotaxis toward phytoplankton drives organic matter partitioning among marine bacteria. *Proc. Natl. Acad. Sci. U.S.A.* **113**, 1576–1581 (2016).
6. J. R. Seymour, S. A. Amin, J. B. Raina, R. Stocker, Zooming in on the phycosphere: The ecological interface for phytoplankton–bacteria relationships. *Nat. Microbiol.* **2**, 17065 (2017).
7. J. M. Sieburth, V. Smetacek, J. Lenz, Pelagic ecosystem structure: Heterotrophic compartments of the plankton and their relationship to plankton size fractions. *Limnol. Oceanogr.* **23**, 1256–1263 (1978).
8. R. M. Macnab, D. E. Koshland, The gradient-sensing mechanism in bacterial chemotaxis. *Proc. Natl. Acad. Sci. U.S.A.* **69**, 2509–2512 (1972).
9. D. A. Brown, H. C. Berg, Temporal stimulation of chemotaxis in *Escherichia coli*. *Proc. Natl. Acad. Sci. U.S.A.* **71**, 1388–1392 (1974).
10. S. Bi, V. Sourjik, Stimulus sensing and signal processing in bacterial chemotaxis. *Curr. Opin. Microbiol.* **45**, 22–29 (2018).
11. H. Berg, E. Purcell, Physics of chemoreception. *Biophys. J.* **20**, 193–219 (1977).
12. P. R. ten Wolde, N. B. Becker, T. E. Ouldridge, A. Mugler, Fundamental limits to cellular sensing. *J. Stat. Phys.* **162**, 1395–1424 (2016).
13. C. Lee, J. L. Bada, Amino acids in equatorial Pacific Ocean water. *Earth Planet. Sci. Lett.* **26**, 61–68 (1975).
14. T. Mora, N. S. Wingreen, Limits of sensing temporal concentration changes by single cells. *Phys. Rev. Lett.* **104**, 248101 (2010).
15. A. M. Hein, D. R. Brumley, F. Carrara, R. Stocker, S. A. Levin, Physical limits on bacterial navigation in dynamic environments. *J. R. Soc. Interface* **13**, 20150844 (2016).
16. D. R. Brumley *et al*., Bacteria push the limits of chemotactic precision to navigate dynamic chemical gradients. *Proc. Natl. Acad. Sci. U.S.A.* **116**, 10792–10797 (2019).
17. W. G. Sprules, M. Munawar, Plankton size spectra in relation to ecosystem productivity, size, and perturbation. *Can. J. Fish. Aquat. Sci.* **43**, 1789–1794 (1986).
18. P. Cermeño, F. Figueiras, Species richness and cell-size distribution: Size structure of phytoplankton communities. *Mar. Ecol. Prog. Ser.* **357**, 79–85 (2008).
19. G. A. Jackson, Simulating chemosensory responses of marine microorganisms: Bacterial chemokinesis. *Limnol. Oceanogr.* **32**, 1253–1266 (1987).
20. J. B. Raina *et al*., Chemotaxis increases metabolic exchanges between marine picophytoplankton and heterotrophic bacteria. *Nat. Microbiol.* **8**, 510–521 (2023).
21. K. Son, F. Menolascina, R. Stocker, Speed-dependent chemotactic precision in marine bacteria. *Proc. Natl. Acad. Sci. U.S.A.* **113**, 8624–8629 (2016).
22. H. Grossart, L. Riemann, F. Azam, Bacterial motility in the sea and its ecological implications. *Aquat. Microb. Ecol.* **25**, 247–258 (2001).
23. J. Johansen, J. Pinhassi, N. Blackburn, U. Zweifel, Å. Hagström, Variability in motility characteristics among marine bacteria. *Aquat. Microb. Ecol.* **28**, 229–237 (2002).
24. T. Kiørboe, H. P. Grossart, H. Ploug, K. Tang, Mechanisms and rates of bacterial colonization of sinking aggregates. *Appl. Environ. Microbiol.* **68**, 3996–4006 (2002).
25. R. B. Blackman, J. W. Tukey, The measurement of power spectra from the point of view of communications engineering–Part I. *Bell Syst. Tech. J.* **37**, 185–282 (1958).
26. S. M. Block, J. E. Segall, H. C. Berg, Impulse responses in bacterial chemotaxis. *Cell* **31**, 215–226 (1982).
27. Y. Tu, T. S. Shimizu, H. C. Berg, Modeling the chemotactic response of *Escherichia coli* to time-varying stimuli. *Proc. Natl. Acad. Sci. U.S.A.* **105**, 14855–14860 (2008).
28. T. Kiørboe, *A Mechanistic Approach to Plankton Ecology* (Princeton University Press, Princeton, NJ, 2008).
29. J. Słomka *et al*., Encounter rates prime interactions between microorganisms. *Interface Focus.* **13**, 20220059 (2023).
30. H. C. Berg, *Random Walks in Biology* (Princeton University Press, 1993).
31. A. C. W. Utne, The effect of turbidity and illumination on the reaction distance and search time of the marine planktivore *Gobiusculus flavescens*. *J. Fish Biol.* **50**, 926–938 (1997).
32. J. M. C. Hutchinson, P. M. Waser, Use, misuse and extensions of "ideal gas" models of animal encounter. *Biol. Rev.* **82**, 335–359 (2007).
33. A. W. Visser, Motility of zooplankton: Fitness, foraging and predation. *J. Plankton Res.* **29**, 447–461 (2007).
34. K. Andersen *et al*., Characteristic sizes of life in the oceans, from bacteria to whales. *Annu. Rev. Mar. Sci.* **8**, 217–241 (2016).
35. E. Gurarie, O. Ovaskainen, Towards a general formalization of encounter rates in ecology. *Theor. Ecol.* **6**, 189–202 (2013).
36. J. C. Maxwell, V., Illustrations of the dynamical theory of gases. Part I. On the motions and collisions of perfectly elastic spheres. *Lond. Edinb. Dublin Philos. Mag. J. Sci.* **19**, 19–32 (1860).
37. M. Smoluchowski, Drei Vorträge über Diffusion, Brownsche Molekularbewegung und Koagulation von Kolloidteilchen. *Z. Phys.* **17**, 557–585 (1916).
38. S. Chandrasekhar, Stochastic problems in physics and astronomy. *Rev. Mod. Phys.* **15**, 1–89 (1943).
39. B. S. Lambert *et al*., A microfluidics-based in situ chemotaxis assay to study the behaviour of aquatic microbial communities. *Nat. Microbiol.* **2**, 1344–1349 (2017).
40. E. E. Clerc *et al*., Strong chemotaxis by marine bacteria towards polysaccharides is enhanced by the abundant organosulfur compound DMSP. *Nat. Commun.* **14**, 8080 (2023).
41. J. E. Segall, M. D. Manson, H. C. Berg, Signal processing times in bacterial chemotaxis. *Nature* **296**, 855–857 (1982).
42. V. Sourjik, H. C. Berg, Binding of the *Escherichia coli* response regulator CheY to its target measured in vivo by fluorescence resonance energy transfer. *Proc. Natl. Acad. Sci. U.S.A.* **99**, 12669–12674 (2002).
43. T. Sagawa *et al*., *E. coli* response to an instantaneously applied chemotactic signal. *Biophys. J.* **107**, 730–739 (2014).
44. J. G. Mitchell *et al*., Long lag times and high velocities in the motility of natural assemblages of marine bacteria. *Appl. Environ. Microbiol.* **61**, 877–882 (1995).
45. J. A. Schramke, S. F. Murphy, W. J. Doucette, W. D. Hintze, Prediction of aqueous diffusion coefficients for organic compounds at 25°C. *Chemosphere* **38**, 2381–2406 (1999).
46. C. E. Spiese, Determination of the diffusion constants of dimethylsulfide and dimethylsulfoniopropionate by diffusion-ordered nuclear magnetic resonance spectroscopy. *Mar. Chem.* **207**, 77–83 (2018).
47. Y. Ma, C. Zhu, P. Ma, K. T. Yu, Studies on the diffusion coefficients of amino acids in aqueous solutions. *J. Chem. Eng. Data* **50**, 1192–1196 (2005).
48. F. J. Massey, The Kolmogorov–Smirnov test for goodness of fit. *J. Am. Stat. Assoc.* **46**, 68–78 (1951).
49. M. M. Mullin, P. R. Sloan, R. W. Eppley, Relationship between carbon content, cell volume, and area in phytoplankton. *Limnol. Oceanogr.* **11**, 307–311 (1966).
50. E. Marañón, P. Cermeño, V. Pérez, Continuity in the photosynthetic production of dissolved organic carbon from eutrophic to oligotrophic waters. *Mar. Ecol. Prog. Ser.* **299**, 7–17 (2005).
51. E. Marañón, P. Cermeño, E. Fernández, J. Rodríguez, L. Zabala, Significance and mechanisms of photosynthetic production of dissolved organic carbon in a coastal eutrophic ecosystem. *Limnol. Oceanogr.* **49**, 1652–1666 (2004).
52. D. L. Kirchman, Growth rates of microbes in the oceans. *Annu. Rev. Mar. Sci.* **8**, 285–309 (2016).
53. C. H. Wigington *et al*., Re-examination of the relationship between marine virus and microbial cell abundances. *Nat. Microbiol.* **1**, 15024 (2016).
54. V. I. Fernandez, Y. Yawata, R. Stocker, A foraging mandala for aquatic microorganisms. *ISME J.* **13**, 563–575 (2019).
55. G. Malaguti, P. R. ten Wolde, Theory for the optimal detection of time-varying signals in cellular sensing systems. *eLife* **10**, e62574 (2021).
56. J. M. Keegstra, F. Carrara, R. Stocker, The ecological roles of bacterial chemotaxis. *Nat. Rev. Microbiol.* **20**, 491–504 (2022).
57. L. T. Nielsen, T. Kiørboe, Foraging trade-offs, flagellar arrangements, and flow architecture of planktonic protists. *Proc. Natl. Acad. Sci. U.S.A.* **118**, e2009930118 (2021).
58. A. Ebrahimi, A. Goyal, O. X. Cordero, Particle foraging strategies promote microbial diversity in marine environments. *eLife* **11**, e73948 (2022).
59. X. Mayali, F. Azam, Algicidal bacteria in the sea and their impact on algal blooms. *J. Eukaryot. Microbiol.* **51**, 139–144 (2004).
60. C. Martínez-Pérez, S. T. Zweifel, R. Pioli, R. Stocker, Space, the final frontier: The spatial component of phytoplankton–bacterial interactions. *Mol. Microbiol.* **122**, 331–346 (2024).
61. R. J. Henshaw *et al*., Metabolites from intact phage-infected Synechococcus chemotactically attract heterotrophic marine bacteria. *Nat. Microbiol.* **9**, 3184–3195 (2024).
62. J. R. Seymour, D. R. Brumley, R. Stocker, J. B. Raina, Swimming towards each other: The role of chemotaxis in bacterial interactions. *Trends Microbiol.* **32**, 640–649 (2024).
63. A. Celani, M. Vergassola, Bacterial strategies for chemotaxis response. *Proc. Natl. Acad. Sci. U.S.A.* **107**, 1391–1396 (2010).
64. L. Xie, T. Altindal, S. Chattopadhyay, X. L. Wu, Bacterial flagellum as a propeller and as a rudder for efficient chemotaxis. *Proc. Natl. Acad. Sci. U.S.A.* **108**, 2246–2251 (2011).
65. Z. Alirezaeizanjani, R. Großmann, V. Pfeifer, M. Hintsche, C. Beta, Chemotaxis strategies of bacteria with multiple run modes. *Sci. Adv.* **6**, eaaz6153 (2020).
66. R. Colin, B. Ni, L. Laganenka, V. Sourjik, Multiple functions of flagellar motility and chemotaxis in bacterial physiology. *FEMS Microbiol. Rev.* **45**, fuab038 (2021).
67. W. Bell, R. Mitchell, Chemotactic and growth response of marine bacteria to algal extracellular products. *Biol. Bull.* **143**, 265–277 (1972).
68. A. J. Platt, K. E. Whalen, Probing the phycosphere: Techniques to study bacteria–phytoplankton interactions. *Integr. Comp. Biol.* **63**, 1509–1519 (2023).
69. R. Snyderman, E. J. Goetzl, Molecular and cellular mechanisms of leukocyte chemotaxis. *Science* **213**, 830–837 (1981).
70. G. Reddy, V. N. Murthy, M. Vergassola, Olfactory sensing and navigation in turbulent environments. *Annu. Rev. Condens. Matter Phys.* **13**, 191–213 (2022).
71. A. Utne-Palm, Visual feeding of fish in a turbid environment: Physical and behavioural aspects. *Mar. Freshw. Behav. Physiol.* **35**, 111–128 (2002).
72. A. M. Hein, F. Carrara, D. R. Brumley, R. Stocker, S. A. Levin, Natural search algorithms as a bridge between organisms, evolution, and ecology. *Proc. Natl. Acad. Sci. U.S.A.* **113**, 9413–9420 (2016).

73. A. M. Hein, B. T. Martin, Information limitation and the dynamics of coupled ecological systems. *Nat. Ecol. Evol.* **4**, 82–90 (2020).
74. J. Rode, M. Novak, B. M. Friedrich, Information theory of chemotactic agents using both spatial and temporal gradient sensing. *PRX Life* **2**, 023012 (2024).
75. H. Mao, P. S. Cremer, M. D. Manson, A sensitive, versatile microfluidic assay for bacterial chemotaxis. *Proc. Natl. Acad. Sci. U.S.A.* **100**, 5449–5454 (2003).
76. M. D. Egbert, X. E. Barandiaran, E. A. Di Paolo, A minimal model of metabolism-based chemotaxis. *PLoS Comput. Biol.* **6**, e1001004 (2010).
77. B. Ni, R. Colin, H. Link, R. G. Endres, V. Sourjik, Growth-rate dependent resource investment in bacterial motile behavior quantitatively follows potential benefit of chemotaxis. *Proc. Natl. Acad. Sci. U.S.A.* **117**, 595–601 (2020).
78. N. Barak-Gavish *et al*., Bacterial lifestyle switch in response to algal metabolites. *eLife* **12**, e84400 (2023).
79. A. K. M. Stubbusch *et al*., Polysaccharide breakdown products drive degradation-dispersal cycles of foraging bacteria through changes in metabolism and motility. *eLife* **13**, RP93855 (2024).
80. L. Li *et al*., Phenotypic variability shapes bacterial responses to opposing gradients. *PRX Life* **2**, 013001 (2024).
81. J. D. Bowen, K. D. Stolzenbach, S. W. Chisholm, Simulating bacterial clustering around phytoplankton cells in a turbulent ocean. *Limnol. Oceanogr.* **38**, 36–51 (1993).
82. A. Visser, B. MacKenzie, Turbulence-induced contact rates of plankton: The question of scale. *Mar. Ecol. Prog. Ser.* **166**, 307–310 (1998).
83. J. R. Taylor, R. Stocker, Trade-offs of chemotactic foraging in turbulent water. *Science* **338**, 675–679 (2012).
84. S. Lange, B. M. Friedrich, Sperm chemotaxis in marine species is optimal at physiological flow rates according theory of filament surfing. *PLoS Comput. Biol.* **17**, e1008826 (2021).
85. P. J. S. Franks, B. G. Inman, J. A. MacKinnon, M. H. Alford, A. F. Waterhouse, Oceanic turbulence from a planktonic perspective. *Limnol. Oceanogr.* **67**, 348–363 (2022).
86. F. Benedetti *et al*., The seasonal and inter-annual fluctuations of plankton abundance and community structure in a North Atlantic marine protected area. *Front. Mar. Sci.* **6**, 214 (2019).
87. N. Haëntjens, E. S. Boss, J. R. Graff, A. P. Chase, L. Karp-Boss, Phytoplankton size distributions in the western North Atlantic and their seasonal variability. *Limnol. Oceanogr.* **67**, 1865–1878 (2022).
88. B. B. Prézelin, "Diel periodicity in phytoplankton productivity" in *The Daily Growth Cycle of Phytoplankton*, T. Berman, H. J. Gons, L. R. Mur, Eds. (Springer, Dordrecht, The Netherlands, 1992), pp. 1–35.
89. T. Takahashi, J. Olafsson, J. G. Goddard, D. W. Chipman, S. C. Sutherland, Seasonal variation of CO_2 and nutrients in the high-latitude surface oceans: A comparative study. *Global Biogeochem. Cycles* **7**, 843–878 (1993).
90. T. Kiørboe, G. A. Jackson, Marine snow, organic solute plumes, and optimal chemosensory behavior of bacteria. *Limnol. Oceanogr.* **46**, 1309–1318 (2001).
91. J. Słomka, U. Alcolombri, E. Secchi, R. Stocker, V. I. Fernandez, Encounter rates between bacteria and small sinking particles. *New J. Phys.* **22**, 043016 (2020).
92. A. E. Zimmerman *et al*., Metabolic and biogeochemical consequences of viral infection in aquatic ecosystems. *Nat. Rev. Microbiol.* **18**, 21–34 (2020).
93. J. P. DeLong, J. L. Van Etten, Z. Al-Ameeli IV, DD Dunigan. Agarkova, The consumption of viruses returns energy to food chains. *Proc. Natl. Acad. Sci. U.S.A.* **120**, e2215000120 (2023).
94. R. Foffi, GradientSensing. GitHub. https://github.com/mastrof/GradientSensing. Deposited 5 June 2024.
95. G. Datseris, J. Isensee, S. Pech, T. Gál, DrWatson: The perfect sidekick for your scientific inquiries. *JOSS* **5**, 2673 (2020).
96. W. M. Kahan, Personal calculator has key to solve any equation f(x)=0. *Hewlett-Packard J.* **30**, 20–26 (1979).
97. D. Lin *et al*., *JuliaStats/Distributions.jl: V0.25.107* (Zenodo, 2024).
98. S. Danisch, J. Krumbiegel, Makie.jl: Flexible high-performance data visualization for Julia. *JOSS* **6**, 3349 (2021).